Application of random phase approximation to vibrational excitations of double-Λ hypernuclei

F. Minato[1] and K. Hagino[2]

[1] *Research group for applied nuclear physics, Japan Atomic Energy Agency, Tokai 319-1195, Japan*
[2] *Department of physics, Tohoku University, Sendai 980-8578, Japan*

(Dated: December 30, 2011)

Using the Hartree-Fock plus random-phase-approximation (HF+RPA), we study the impurity effect of Λ hyperon on the collective vibrational excitations of double-Λ hypernuclei. To this end, we employ a Skyrme-type ΛN and ΛΛ interactions for the HF calculations, and the residual interactions for RPA derived with the same interactions. We find that inclusion of two Λ hyperons in ^{16}O shifts the energy of the collective states towards higher energies. In particular, the energy of the giant monopole resonance of $^{18}_{\Lambda\Lambda}$O, as well as that of $^{210}_{\Lambda\Lambda}$Pb, becomes larger. This implies that the effective incompressibility modulus increases due to the impurity effect of Λ particle, if the β-stability condition is not imposed.

PACS numbers: 21.80.+a,21.60.Jz, 21.10.Re,23.20.-g

I. INTRODUCTION

Information on the interaction between a Λ hyperon and a nucleon deepens our understanding of baryon-baryon forces and the equation of state (EOS) of nuclear matter. In principle, the interaction between two particles can be investigated with a measurement of their scattering. However, due to the short life-time of Λ hyperon, it has yet been difficult to perform a direct scattering experiment of nucleon and Λ hyperon. Therefore, the ΛN interaction has been mainly investigated by γ spectroscopy of single-Λ hypernuclei [1–5]. Such measurements have revealed the Λ-impurity effect, that is, the change of several properties of atomic nuclei, such as excitation energies and transition probabilities of γ-ray, due to an addition of Λ particle. Apparently, high-resolution γ-ray measurements are vital in investigating Λ hypernuclei. In addition to the existing experimental data, research projects currently planned at the J-PARC facility using new Ge detector arrays (Hyperball-J)[6] aim at obtaining new data on the low-lying energy level scheme of Λ hypernuclei in the *sd* shell region, that will lead to further understanding of the ΛN and ΛΛ interactions.

Several theoretical calculations have been carried out to analyze the relation between low-lying energy levels of single-Λ hypernuclei and the ΛN interaction [7–14]. These calculations have not only contributed to identification of energy level schemes of single-Λ hypernuclei, but have also predicted the Λ-impurity effect on the structure of single-Λ hypernuclei, *e.g.*, shrinkage of the radius of $^{7}_{\Lambda}$Li from ^{6}Li[10], which was subsequently observed experimentally [1].

Besides single-Λ hypernuclei, double-Λ hypernuclei have also been studied both experimentally and theoretically. Similar to the ΛN interaction, information on the ΛΛ interaction can be deduced from observation of γ-rays emitted from double-Λ hypernuclei. However, until now double-Λ hypernuclei have been produced only in an emulsion, and at present emitted γ-rays are difficult to detect experimentally with high precision. In addition, so far observed double-Λ hypernuclei in the emulsion have been limited to five cases($^{6}_{\Lambda\Lambda}$He and $^{10-13}_{\Lambda\Lambda}$B [15, 16]), and the experimental data have been scarce. Therefore the theoretical approaches make an important tool to assess the Λ impurity effect on the structure of double-Λ hypernuclei as well as appropriate selection of a target nucleus for future experiments. Theoretically, the double-Λ hypernuclei have been investigated within the frameworks of ab-initio few body model[17], shell model[18] and cluster model[19]. However, these theoretical approaches demand a huge computational power, and they may be difficult to apply to heavy hypernuclei.

In order to study systematically the Λ-impurity effect, from light to heavy nuclei, a Hartree-Fock (HF) plus random-phase-approximation (RPA) method provides one of the most suitable tools. This approach has been applied to study vibrational excitations of normal nuclei (without hyperons) throughout the nuclear chart, starting with a single energy functional applicable in the whole range of the nuclear chart. In particular, the RPA has been successfully applied to descriptions of giant resonances of atomic nuclei. See Refs.[20–23] for earlier applications of Tamm-Dancoff approximation to (K^-,π^-) and (π^+,K^+) reactions, and of an RPA-like model to single-particle spectra of single-Λ hypernuclei. So far, the mean field approach has been extended to Λ hypernuclei in order to study the ground state properties [24–29], the potential energy surface in the deformation plane [30–32] and fission barrier heights [33]. Concerning excited states, the low-lying excited states of $^{25}_{\Lambda}$Mg have recently been calculated with a 5-dimensional (5D) collective Bohr Hamiltonian on the basis of the Skyrme-Hartree-Fock method [34] (see also Ref.[13] for a recent application of anti-symmetrized molecular dynamics to the $^{25}_{\Lambda}$Mg hypernucleus). Although the Bohr Hamiltonian approach can handle a large amplitude collective motion, it is much easier to employ the RPA approach to describe collective vibrations with several multipolarities, including giant resonances as well.

In this paper, we extend the Skyrme-HF plus RPA (SHF+RPA) scheme to hypernuclei. Skyme-type ΛN and ΛΛ interactions, similarly to the Skyrme nucleon-nucleon interaction, are used in this work. The residual interactions for RPA are derived self-consistently from the second derivative of the energy functional with respect to densities. In this study, we shall focus on the double-Λ hypernuclei rather than single-Λ hypernuclei, partly because the description is much simpler due to the time-reversal symmetry. The Λ-impurity effect is expected to be stronger in double-Λ hypernuclei, and such calculations will provide the upper limit of the impurity effect for single-Λ hypernuclei.

The paper is organized as follows. In Sec. II, we describe the formalism of the SHF+RPA for hypernuclei. In Sec. III, we apply the SHF+RPA method to ${}^{18}_{\Lambda\Lambda}$O hypernuclei and present the results for the strength distributions and the transition densities for the isoscalar giant monopole resonance (IS 0^+), the electric dipole (E1), quadrupole (E2) and octupole (E3) transitions. We also calculate the isoscalar giant monopole resonance of ${}^{210}_{\Lambda\Lambda}$Pb hypernucleus and discuss the nuclear incompressibility in the presence of Λ hyperon. We give a summary of the paper in Sec. IV.

II. RPA FOR HYPERNUCLEI

In order to describe the ground state and excited states of double-Λ hypernuclei, we adopt the Skyrme-type zero-range force for the ΛN and $\Lambda\Lambda$ interactions. The ΛN and 3-body ΛNN interactions of this type were first introduced by Rayet as[24],

$$\begin{aligned} v_{\Lambda N}(\boldsymbol{r}_\Lambda - \boldsymbol{r}_N) &= t_0^\Lambda(1 + x_0^\Lambda P_\sigma)\delta(\boldsymbol{r}_\Lambda - \boldsymbol{r}_N) \\ &+ \frac{1}{2}t_1^\Lambda\left(\boldsymbol{k'}^2\delta(\boldsymbol{r}_\Lambda - \boldsymbol{r}_N) + \delta(\boldsymbol{r}_\Lambda - \boldsymbol{r}_N)\boldsymbol{k}^2\right) \\ &+ t_2^\Lambda \boldsymbol{k'}\delta(\boldsymbol{r}_\Lambda - \boldsymbol{r}_N)\cdot\boldsymbol{k} + iW_0^\Lambda \boldsymbol{k'}\delta(\boldsymbol{r}_\Lambda - \boldsymbol{r}_N)\cdot(\sigma\times\boldsymbol{k}), \end{aligned} \tag{1}$$

and

$$v_{\Lambda NN}(\boldsymbol{r}_\Lambda, \boldsymbol{r}_{N_1}, \boldsymbol{r}_{N_2}) = t_3^\Lambda\delta(\boldsymbol{r}_\Lambda - \boldsymbol{r}_{N_1})\delta(\boldsymbol{r}_\Lambda - \boldsymbol{r}_{N_2}), \tag{2}$$

respectively. In a similar way, Lanskoy introduced the ΛΛ interaction as [26],

$$\begin{aligned} v_{\Lambda\Lambda}(\boldsymbol{r}_{\Lambda_1} - \boldsymbol{r}_{\Lambda_2}) &= \lambda_0\delta(\boldsymbol{r}_{\Lambda_1} - \boldsymbol{r}_{\Lambda_2}) \\ &+ \frac{1}{2}\lambda_1\left(\boldsymbol{k'}^2\delta(\boldsymbol{r}_{\Lambda_1} - \boldsymbol{r}_{\Lambda_2}) + \delta(\boldsymbol{r}_{\Lambda_1} - \boldsymbol{r}_{\Lambda_2})\boldsymbol{k}^2\right) \\ &+ \lambda_2\boldsymbol{k'}\delta(\boldsymbol{r}_{\Lambda_1} - \boldsymbol{r}_{\Lambda_2})\cdot\boldsymbol{k} \\ &+ \lambda_3\left[\rho_N\left(\frac{\boldsymbol{r}_{\Lambda_1} + \boldsymbol{r}_{\Lambda_2}}{2}\right)\right]^{\alpha_\Lambda}\delta(\boldsymbol{r}_{\Lambda_1} - \boldsymbol{r}_{\Lambda_2}). \end{aligned} \tag{3}$$

The operator $\boldsymbol{k'} = -(\boldsymbol{\nabla}_1 - \boldsymbol{\nabla}_2)/2i$ acts on the left hand side while $\boldsymbol{k} = (\boldsymbol{\nabla}_1 - \boldsymbol{\nabla}_2)/2i$ acts on the right hand side. $\rho_N(\boldsymbol{r})$ is the density distribution for the nucleons. The last term in Eq.(3) corresponds to the three-body $\Lambda\Lambda N$ interaction, which originates mainly from the $\Lambda\Lambda - \Xi N$ coupling [35].

Together with the Skyrme NN interaction[36], the total energy $E_{\rm tot}$ in the Hartree-Fock approximation is given by

$$E_{\rm tot} = E_N + E_\Lambda, \tag{4}$$

where

$$E_N = \int H_N(\boldsymbol{r})\, d\boldsymbol{r}, \tag{5}$$

is the energy for the core nucleus without Λ hyperons while

$$E_\Lambda = \int \left[H_{N\Lambda}(\boldsymbol{r}) + H_{\Lambda\Lambda}(\boldsymbol{r})\right] d\boldsymbol{r}, \tag{6}$$

is due to the ΛN and $\Lambda\Lambda$ interactions (see Appendix A). The kinetic energy density for Λ particles is included in the energy density $H_{N\Lambda}(\boldsymbol{r})$.

The SHF equations are obtained by taking variation of the total energy $E_{\rm tot}$ with respect to the densities for neutrons, protons and Λ hyperons. These are given as

$$\left(-\boldsymbol{\nabla}\cdot\frac{\hbar^2}{2m_b^*(\boldsymbol{r})}\boldsymbol{\nabla} + U_{bN}(\boldsymbol{r}) + U_{b\Lambda}(\boldsymbol{r})\right)\phi_b(\boldsymbol{r}) = \epsilon_b\phi_b(\boldsymbol{r}), \tag{7}$$

where the index b refers to proton, neutron or Λ, and ϵ_b is the single-particle energy. The explicit forms for the mean-field potentials $U_{bN}(\boldsymbol{r})$ and $U_{b\Lambda}(\boldsymbol{r})$, and the effective mass $m_b^*(\boldsymbol{r})$ are given in Appendix A.

After we construct the ground state in the Hartree-Fock approximation, we describe excited states with RPA as a linear superposition of 1 particle-1 hole (1p1h) configurations. That is, the excitation operator $Q_k^\dagger$ for the k-th RPA phonon is assumed to be,

$$Q_k^\dagger = \sum_{p,h\in n,p,\Lambda}\left(X_{ph}^{(k)}a_p^\dagger a_h - Y_{ph}^{(k)}a_h^\dagger a_p\right), \tag{8}$$

where $X_{ph}^{(k)}$ and $Y_{ph}^{(k)}$ are the forward and backward amplitudes, respectively. $a_p^\dagger$ and $a_h^\dagger$ are the creation operators for a particle state p and for a hole state h, respectively. The excitation energy E_k is obtained by diagonalizing the 2ν-dimensional RPA equation,

$$\begin{pmatrix} A & B \\ -B^* & -A^* \end{pmatrix}\begin{pmatrix} X^{(k)} \\ Y^{(k)} \end{pmatrix} = E_k\begin{pmatrix} X^{(k)} \\ Y^{(k)} \end{pmatrix}, \tag{9}$$

where ν is the number of 1p1h configurations. Here, A and B are RPA matrices given by,

$$\begin{aligned} A_{ph,p'h'} &= (\epsilon_p - \epsilon_h)\delta_{pp'}\delta_{hh'} + v_{ph'hp'} \\ B_{ph,p'h'} &= v_{pp'hh'}, \end{aligned} \tag{10}$$

where v is the residual interaction derived from the energy functional, $E_{\rm tot}$. The formalism is almost the same as the standard RPA found *e.g.,* in Refs.[37, 38], but

the particle-hole configurations run over not only protons and neutron but also Λ hyperons. The interaction matrix elements $v_{ph'hp'}$ and $v_{pp'hh'}$ include the ΛN and ΛΛ interactions as well as the NN interaction (see Appendix B).

The external fields for electric multipole excitations with multipolarities $L \neq 0$ and 1 are defined as

$$\hat{F}_{EL} = e \sum_{i\in p} r_i^L Y_{LM}(\hat{r}_i), \tag{11}$$

while that for the "isoscalar" monopole transition is

$$\hat{F}_{0^+} = \sum_{i\in p,n,\Lambda} r_i^2. \tag{12}$$

For the electric dipole response, we take into account the center of mass motion of the whole hypernucleus and use the operator

$$\begin{aligned}\hat{F}_{E1} &= e\sum_{i\in p}(r_i Y_{1M}(\hat{r}_i) - R Y_{1M}(\boldsymbol{R})),\\ &= e\frac{Nm_N + N_\Lambda m_\Lambda}{M}\sum_{i\in p} r_i Y_{1M}(\hat{r}_i)\\ &- e\frac{Z}{M}\left(m_N\sum_{i\in n} r_i Y_{10}(\hat{r}_i) + m_\Lambda \sum_{i\in\Lambda} r_i Y_{10}(\hat{r}_i)\right),\end{aligned} \tag{13}$$

where

$$\boldsymbol{R} = \frac{1}{M}\left(m_N\sum_{i\in n,p}\boldsymbol{r}_i + m_\Lambda\sum_{i\in\Lambda}\boldsymbol{r}_i\right), \tag{14}$$

is the center of mass of the hypernucleus, and $M \equiv m_N(Z+N) + m_\Lambda N_\Lambda$ is the total mass, $m_N = (m_p + m_n)/2 = 938.92$ MeV/c^2 and $m_\Lambda = 1115.68$ MeV/c^2 being the mass of nucleon and Λ hyperon, respectively. N, Z and N_Λ are the number of neutron, proton and Λ hyperon, respectively.

III. RESULTS

A. single-particle level of $^{18}_{\Lambda\Lambda}$O

We now numerically solve the RPA equation and discuss the collective excitations of double-Λ hypernuclei. Before we show the results for multipole vibrations, we first discuss the single particle levels of double-Λ hypernucleus $^{18}_{\Lambda\Lambda}$O and ^{16}O, which will help to understand the Λ-impurity effect on the giant resonances. To this end, we assume spherical symmetry, and solve the SHF equation in the coordinate space with a grid size of dr=0.1 fm. We use the SkM* parameter set for NN interaction [39], while the No.5 parameter set in Ref.[25] for the ΛN interaction, whose parameters were determined by fitting the Hartree-Fock calculations to the experimental binding energies of single-Λ hypernuclei[25]. For the ΛΛ interaction, we use the SΛΛ1 parameter set evaluated by Lanskoy[26]. This parameter set was obtained by fitting to the ΛΛ bond energy [26], $\Delta B_{\Lambda\Lambda} = B_{\Lambda\Lambda} - 2B_\Lambda$, where B_Λ is the one-Λ hyperon separation energy from a $^{A+1}_{\Lambda}$Z hypernucleus and $B_{\Lambda\Lambda}$ is the two-Λ hyperon separation energy of $^{A+2}_{\Lambda\Lambda}$Z. As we will show in the next subsection, the dependence of giant resonances on a choice of parameter sets for the ΛN and the ΛΛ interactions is weak, and any significant change in the results is not obtained even if we use different parameter sets for the interactions.

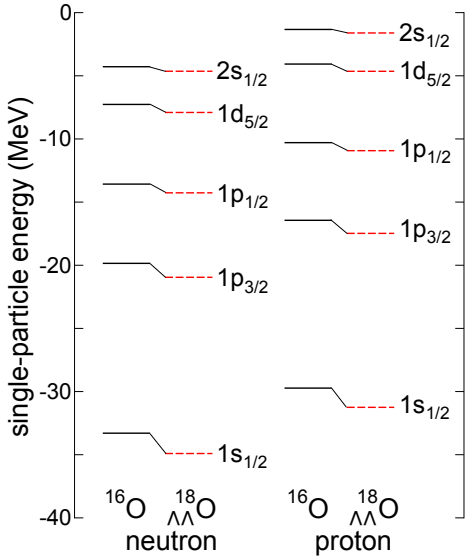

FIG. 1: (Color online) Neutron and proton single-particle levels of ^{16}O (the solid lines) and $^{18}_{\Lambda\Lambda}$O (the dashed lines) obtained with the Skyrme-Hartree-Fock method.

Figure 1 shows the neutron and proton single-particle levels of the ^{16}O (the solid lines) and the $^{18}_{\Lambda\Lambda}$O (the dashed lines). The single-particle energies of the $^{18}_{\Lambda\Lambda}$O hypernucleus are smaller than those of ^{16}O, since the depths of the central part of the mean-field potentials are deepened both for protons and neutrons due to the attractive ΛN interaction, as shown in Fig.2 of Ref.[27]. The lowest level ($1s_{1/2}$) is the most sensitive to the addition of Λ particles, for which the single particle levels are shifted by $\Delta\epsilon_n = -1.4$ MeV for neutron and $\Delta\epsilon_p = -1.3$ MeV for proton. This Λ-impurity effect becomes weaker as the energy of a single-particle state increases. If the continuum spectra are discretized within a large box, the difference of single-particle energies between the ^{16}O and the $^{18}_{\Lambda\Lambda}$O nuclei is much smaller as compared to the bound levels. Consequently, in the independent-particle approximation, the excitation energies increase relatively in the double-Λ hypernucleus as compared to those of the normal nucleus. In the next subsections, we will see that this is the case even in the presence of the residual particle-hole interaction.

TABLE I: The excitation energies and the electromagnetic transition probabilities, $B(E2)$ and $B(E3)$, for the first 2^+ and 3^- states of ^{16}O and $^{18}_{\Lambda\Lambda}$O nuclei obtained with the Skyrme-HF+RPA method.

	2^+_1 state		3^-_1 state	
nucleus	E (MeV)	$B(E2)$ (e^{2}fm^4)	E (MeV)	$B(E3)$ (e^{2}fm^6)
^{16}O	13.1	0.726	6.06	91.1
$^{18}_{\Lambda\Lambda}$O	13.8	0.529	6.32	67.7

B. Low-lying excitations

We next solve the RPA equation in order to discuss collective excitations of the $^{18}_{\Lambda\Lambda}$O hypernucleus. To this end, we discretize the single-particle continuum states with the box boundary condition with the box size of 16.0 fm. We take into account the continuum states up to ϵ=30 MeV, and consider the 1p1h configurations whose unperturbed energy, $\epsilon_p - \epsilon_h$, is smaller than 60 MeV. For the residual interactions, we neglect the Coulomb and the spin-orbit terms for simplicity, although we include all the other terms self-consistently. Therefore, our RPA calculations are not fully self-consistent, and the spurious translational motion appears at a finite excitation energy. In order to recover effectively the self-consistency, we introduce a scaling factor f to the residual interaction v_{res} so as to produce the spurious translational mode at zero energy.

Table I shows the results of such RPA calculations for the lowest quadrupole and the octupole states of ^{16}O and $^{18}_{\Lambda\Lambda}$O. For both the 2^+_1 and 3^-_1 states, the impurity effects of Λ particles slightly reduces the collectivity, that is, the excitation energies are increased while the electromagnetic transition probabilities are decreased by 26-28 %. The increase of the excitation energies is consistent with the increase of unperturbed particle-hole energies discussed in the previous subsection.

C. Giant resonances

The RPA method has been successfully applied to giant resonances of the normal nuclei. We therefore apply it in this subsection to the giant resonances of the double-Λ hypernucleus $^{18}_{\Lambda\Lambda}$O, although they may not be easy to access experimentally at present. The top, the middle, and the bottom panels of Fig. 2 show the strength distributions for the electric dipole (E1), quadrupole (E2) and octupole (E3) excitations, respectively, weighted by the Lorentzian function with a width of 1.0 MeV. The solid and the dashed lines denote the results for the $^{18}_{\Lambda\Lambda}$O and ^{16}O nuclei, respectively. In order to assess the role of Λ hyperon, we also show the results for the $^{18}_{\Lambda\Lambda}$O hypernuclei in which the ΛN and $\Lambda\Lambda$ interactions are taken into account only in the ground state, that is, the results obtained by switching off the residual ΛN and $\Lambda\Lambda$ interactions (the dotted lines). The figure indicates that

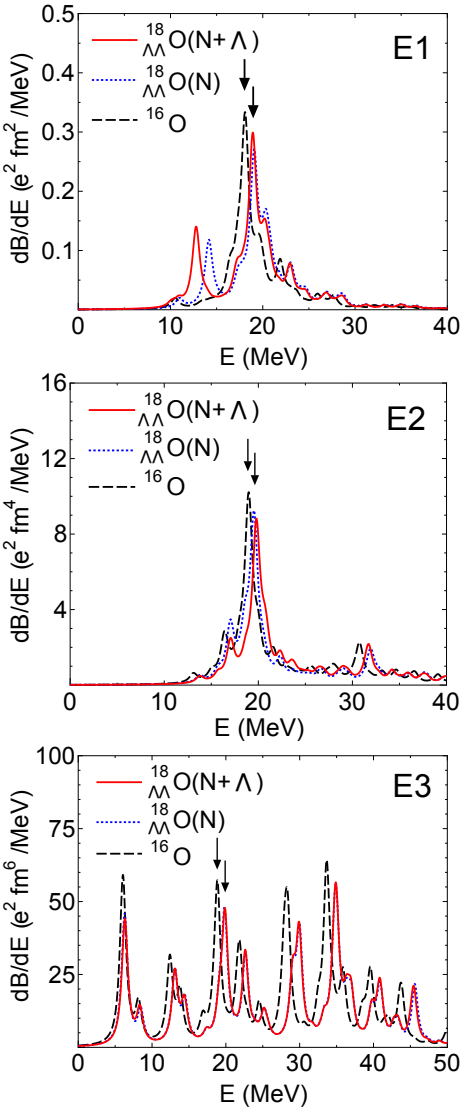

FIG. 2: (Color online) The strength distributions for the electric dipole (E1, the top panel), the electric quadrupole (E2, the middle panel) and the electric octupole (E3, the bottom panel) excitations of the ^{16}O nucleus (the dashed lines) and of the double-Λ hypernucleus $^{18}_{\Lambda\Lambda}$O (the solid and the dotted lines). The solid lines are obtained by including the residual NN, ΛN and $\Lambda\Lambda$ interactions, while the dotted lines are obtained by including only the residual NN interactions. The strength distributions are weighted by the Lorentzian function with a width of 1.0 MeV. For the peaks indicated by the arrows, the transition densities are shown in Fig.3.

the addition of the Λ hyperons shifts the peaks of the strength functions towards high energy for all the modes of excitations. This is similar to the results for the low-lying modes of excitations discussed in the previous subsection, and is again caused mainly by the change of the single-particle energies. On the other hand, the difference between the solid and the dotted lines is relatively small, except for the low-lying dipole state at E = 12.8 MeV. We have confirmed that the strength functions remain

TABLE II: The centroid energy $\overline{E}$ for the E1, E2 and E3 modes of excitations for ^{16}O and $^{18}_{\Lambda\Lambda}$O nuclei. Those are given in units of MeV, and the results of both the unperturbed (HF) and the perturbed (RPA) calculations are shown. $\delta\overline{E}$ denotes the difference of the centroid energies between $^{18}_{\Lambda\Lambda}$O and ^{16}O. The values in the parentheses for the E1 mode are the results obtained by excluding the contribution of the low-lying peak at $E = 12.8$ MeV.

		E1	E2	E3
(HF)	^{16}O	13.76	25.57	26.53
	$^{18}_{\Lambda\Lambda}$O	14.34	26.63	27.74
	$\delta\overline{E}$	+0.58	+1.06	+1.21
(RPA)	^{16}O	19.92	19.55	22.32
	$^{18}_{\Lambda\Lambda}$O	19.68 (20.95)	20.09	24.05
	$\delta\overline{E}$	−0.24 (+1.03)	+0.54	+1.73

almost the same, including the low-lying dipole state, even if other parameter sets for the ΛN and $\Lambda\Lambda$ interactions are employed. This suggests that the main effect of Λ particles on the collective vibrational excitations is indeed attributed to the change in the single-particle energies, rather than the residual ΛN and $\Lambda\Lambda$ interactions, although the low-lying dipole state may require a separate analysis (see Fig. 4 below).

In order to see the Λ-impurity effect quantitatively, we show in Table II the centroid energy defined as $\overline{E} = m_1/m_0$, where m_k is k-th energy-weighted sum-rule,

$$m_k = \sum_\nu (E_i)^k \left| \langle i|F|0\rangle \right|^2, \tag{15}$$

for the unperturbed (HF) and the perturbed (RPA) strength functions. We also list the difference of the centroid energy, $\delta\overline{E}$, between the $^{18}_{\Lambda\Lambda}$O and the ^{16}O nuclei. The values in the parentheses for the RPA E1 response are the results obtained by excluding the contribution of the low-lying dipole peak at $E = 12.8$ MeV. As is expected, the centroid energies $\overline{E}$ for the HF calculations shift to higher energies when the Λ hyperons are added to ^{16}O. For the E2 and E3 responses, this remain the same even if the residual interactions are taken into account in RPA. For the E1 response, the energy shift is negative, but it turs to positive if the low-lying peak is excluded. As we will show below, this low-lying peak corresponds to the dipole motion of a Λ hyperon against the core nucleus. We thus conclude that the Λ hyperons generally increases the centroid energy for collective motions of the core nucleus, not only for the quadrupole and the octupole states but also for the dipole states.

Figure 3 shows the transition densities for the giant dipole and quadrupole resonances and for the high-lying octupole state, which are indicated by the arrows in Fig.2. The top, the middle and the bottom panels denote the transition densities for the neutrons, the protons and the Λ hyperons, respectively. Those transition densities are computed as

$$\delta\rho_i(r) = \sum_{ph} (X^{(i)}_{ph} + (-1)^L Y^{(i)}_{ph}) \times \varphi_p(r)\varphi_h(r)\langle j_p l_p||Y_L||j_h l_h\rangle, \tag{16}$$

where j_i, l_i are the total and the orbital angular momenta for a single-particle state i, respectively, while $\varphi_i(r)$ is the radial part of the wave function, normalized as $\int_0^\infty \varphi_i^*(r)\varphi_i(r)\, r^2 dr = 1$. The peaks of the transition densities for the neutrons and protons slightly move to a small distance and are shifted towards inside for all the multipolarities when two Λ hyperons are added. The amplitude of the transition density for the Λ hyperons is about $1/10 - 1/100$ smaller than that for the protons and neutrons, so that the Λ hyperons do not contribute much to these giant resonances. For the E2 and E3 states, the neutrons and the protons oscillate in phase as is expected for isoscalar motions, while they oscillate out of phase for the E1 state (*i.e.,* the isovector motion). In addition, the Λ hyperons oscillate in phase with the protons and the neutrons for the E2 and the E3 modes, while they oscillate in phase with the protons for the E1 mode. When the Coulomb force is turned off completely, that is, when the single-particle levels for the protons are identical to those for the neutrons, the amplitude of the E1 transition density for the Λ hyperons vanish.

The low-lying dipole state at $E = 12.8$ MeV deserves a special attention. This peak appears only when the Λ hyperons are added to the ^{16}O nucleus, and a similar peak does not seen in other modes of excitations. Figure 4 shows the transition density for this state. In contrast to the giant resonance shown in Fig.3, the amplitude of the transition density for the Λ hyperons is higher than that for the protons and the neutrons. The strongest RPA amplitude, $\xi \equiv X^2 - Y^2$, contributing to this peak is the $[1p\,(1s)^{-1}]$ configuration of the Λ particles ($\xi = 0.873$). The total RPA amplitudes for the neutrons and the protons are small ($\xi = 0.050$ for the neutrons and $\xi = 0.071$ for the protons), and these values become entirely zero when the ΛN interaction is switched off. The neutrons and the protons oscillate in phase, and the Λ particles oscillate out of phase with the nucleons. We can thus interpret this mode as a dipole oscillation of the Λ particles against the core nucleus ^{16}O, similar to the soft dipole motion of a valence neutron in halo nuclei [40].

D. Giant monopole resonance and incompressibility

Giant monopole resonances, the so called "breathing mode", are intimately related to the incompressibility of nuclear matter [41–47], which plays an important role in neutron stars. It has been shown that the EOS of infinite nuclear matter is softened when hyperons(Λ, Ξ, Σ) emerge at high densities, and as a consequence the maximum mass of neutron stars becomes smaller [48–50]. It

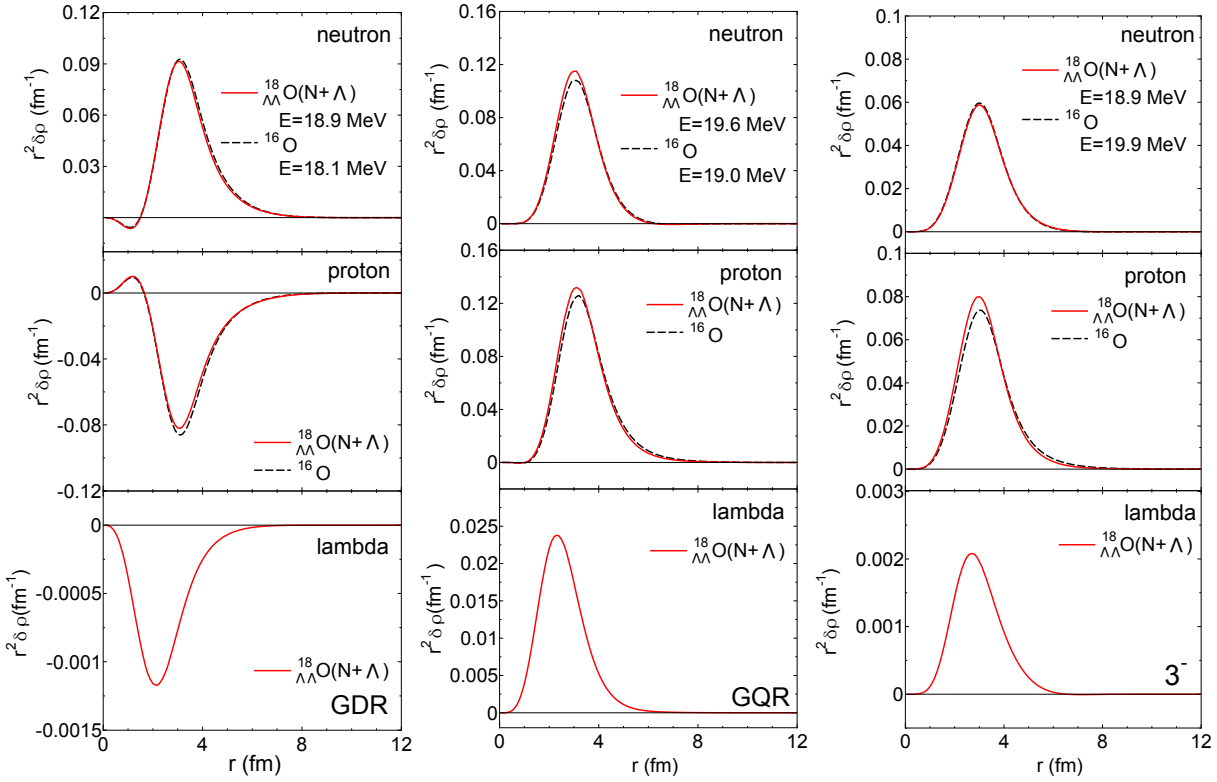

FIG. 3: (Color online) The transition densities for the giant dipole (the left panel) and the giant quadrupole (the middle panel) resonances and for the high-lying octupole state (the right panel) in ${}^{18}_{\Lambda\Lambda}$O (the solid lines) and ^{16}O (the dashed lines). The corresponding states are denoted by the arrows in Fig. 2. The top, the middle, and the bottom panels denote the transition densities for the neutrons, the protons and the Λ hyperons, respectively.

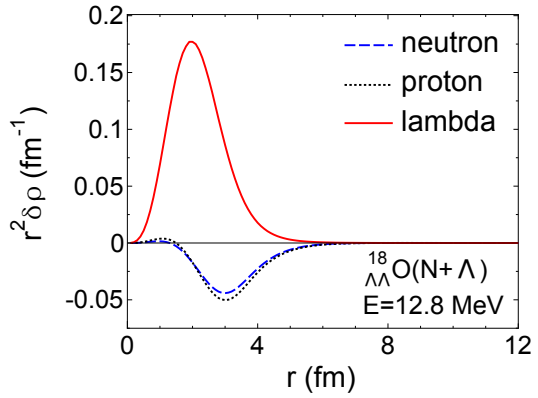

FIG. 4: (Color online) The transition density for the low-lying E1 state at $E = 12.8$ MeV in the ${}^{18}_{\Lambda\Lambda}$O hypernucleus. The dashed, the dotted, and the solid lines show the contributions of the neutrons, the protons, and the Λ hyperons, respectively.

is thus of interest to investigate the Λ-impurity effect of giant monopole resonances in finite nuclei.

Figure 5 shows the strength function for the isoscalar monopole responses of ^{16}O and ${}^{18}_{\Lambda\Lambda}$O nuclei. The meaning of each line is the same as in Fig. 2. For a comparison, the figure also shows the strength function for ^{208}Pb and ${}^{208}_{\Lambda\Lambda}$Pb. As in the other multipolarities discussed in the previous subsection, the strength distributions are shifted towards high energies when Λ hyperons are added, and also the difference between the solid and the dotted lines is small, indicating that the residual ΛN and $\Lambda\Lambda$ interactions play a minor role.

Figure 6 shows the transition densities for the giant monopole resonances corresponding to the states indicated by the arrows in the Fig.5 (that is, those states at $E = 22.2$ MeV and 21.1 MeV for ${}^{18}_{\Lambda\Lambda}$O and ^{16}O, respectively, and at 14.6 MeV and 14.2 MeV for ${}^{210}_{\Lambda\Lambda}$Pb and ^{208}Pb, respectively). The meaning of each line is the same as in Fig. 3. For the oxygen nuclei, when Λ hyperons are added, the amplitude of the transition density for the neutrons decreases by about 20% while that for the protons remains almost the same. The amplitude of the Λ transition density is about 10 times smaller than that of the nucleons. It is interesting to notice that the Λ hyperons oscillate out of phase with the nucleons. These features are qualitatively the same for the lead nuclei as well, although the changes in the transition densities are much smaller compared to the oxygen isotopes.

According to Blaizot, the effective incompressibility modulus K_A for finite nuclei without Λ hyperons is defined as [41],

$$K_A = \frac{m_N}{\hbar^2}\mathcal{E}^2\langle r^2\rangle, \tag{17}$$

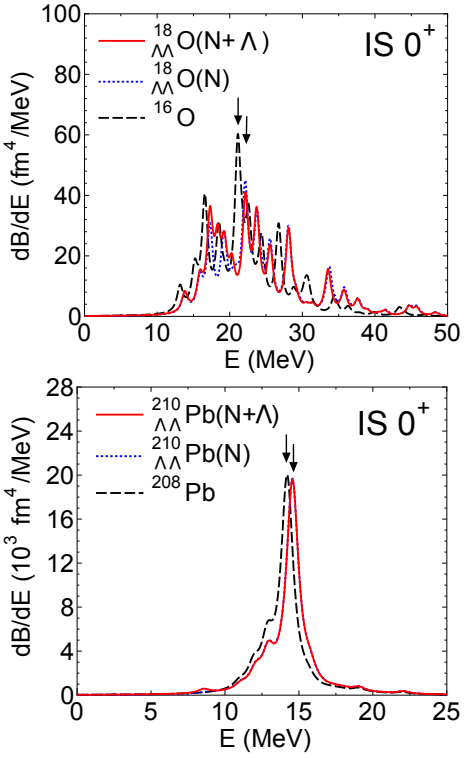

FIG. 5: (Color online) The strength distributions for the isoscalar monopole mode for the ^{16}O and $^{18}_{\Lambda\Lambda}$O nuclei (the top panel) and for the ^{208}Pb and $^{210}_{\Lambda\Lambda}$Pb nuclei (the bottom panel). The meaning of each line is the same as in Fig. 2.

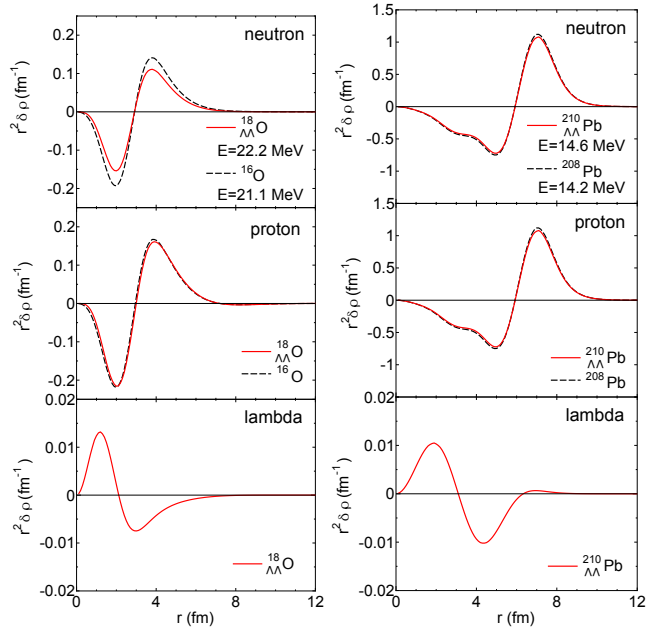

FIG. 6: (Color online) The transition densities for the isoscalar giant monopole resonances of $^{18}_{\Lambda\Lambda}$O (the left panels) and $^{210}_{\Lambda\Lambda}$Pb (the right panels), with comparisons to the transition densities for ^{16}O and ^{208}Pb. The meaning of each line is the same as in Fig. 3.

TABLE III: Properties of the isoscalar monopole responses obtained with the Skyrme HF+RPA method. $\overline{E}_{0^+}$ is the centroid energy, and $\mathcal{E}$ is defined as $\mathcal{E} = \sqrt{m_1/m_{-1}}$. $\sqrt{\langle r^2\rangle_{\rm n+p}}$ and $\sqrt{\langle r^2\rangle}$ are the root mean square radii for the core nuclei and that for the total densities, respectively. K_A is the effective nuclear incompressibility defined by Eqs. (17) and (18).

	$\overline{E}_{0^+}$(MeV)	$\mathcal{E}$(MeV)	$\sqrt{\langle r^2\rangle_{\rm n+p}}$	$\sqrt{\langle r^2\rangle}$(fm)	K_A(MeV)
^{16}O	22.4	21.7	2.68	2.68	81.6
$^{18}_{\Lambda\Lambda}$O	24.3	23.5	2.64	2.58	90.0
^{208}Pb	14.1	14.0	5.56	5.56	146
$^{210}_{\Lambda\Lambda}$Pb	14.5	14.4	5.55	5.53	153

where $\sqrt{\langle r^2\rangle}$ is the root mean square radius, and $\mathcal{E}^2 = m_1/m_{-1}$ (see Eq. (15) for the definition of the k-th energy-weighted sum-rule, m_k). When the Λ hyperons are present, this formula is modified as,

$$K_A = \frac{m_N}{\hbar^2}\mathcal{E}^2\langle r^2\rangle\left(\frac{N+Z}{A}\frac{\langle r^2\rangle_{\rm n+p}}{\langle r^2\rangle} + \frac{m_N N_\Lambda}{m_\Lambda A}\frac{\langle r^2\rangle_\Lambda}{\langle r^2\rangle}\right)^{-1}, \quad (18)$$

where we have used Eqs. (3.45) and (3.47) in Ref.[41] and the energy-weighted sum-rule for the isoscalar monopole transition,

$$m_1(L=0) = \frac{2\hbar^2}{m_N}(N+Z)\langle r^2\rangle_{\rm n+p} + \frac{2\hbar^2}{m_\Lambda}N_\Lambda\langle r^2\rangle_\Lambda. \quad (19)$$

In Eq. (18), $\sqrt{\langle r^2\rangle}_{\rm n+p}$ is the root mean square radius of the core nucleus. Notice that Eq. (18) is reduced to Eq.(17) when $N_\Lambda = 0$. In Table III, we list the centroid energy $\overline{E}_{0^+}$, $\mathcal{E}$ for the isoscalar monopole modes, the root-mean-square radii, $\sqrt{\langle r^2\rangle}$ and $\sqrt{\langle r^2\rangle_{\rm n+p}}$, and the effective incompressibility, K_A, calculated according to Eqs. (17) and (18). When Λ hyperons are added, the centroid energies increase by 1.9 MeV for ^{16}O and 0.4 MeV for ^{208}Pb, and the rms radii for the core nucleus, $\sqrt{\langle r^2\rangle_{\rm n+p}}$, decrease by 0.04 fm for ^{16}O and 0.01 fm for ^{208}Pb. As we have shown, the increase of the centroid energies is mainly due to the change of single-particle levels, and the residual ΛN and $\Lambda\Lambda$ interactions give only a minor effect. The decrease of the rms radii is attributed to the attractive ΛN interaction, that is, the shrinkage effect of Λ hyperons. The effective incompressibility, K_A, increases for both the nuclei studied when Λ hyperons are added.

The increase of the effective incompressibility should reflect the properties of infinite nuclear matter. In order to assess this, Fig. 7 shows the binding energy per

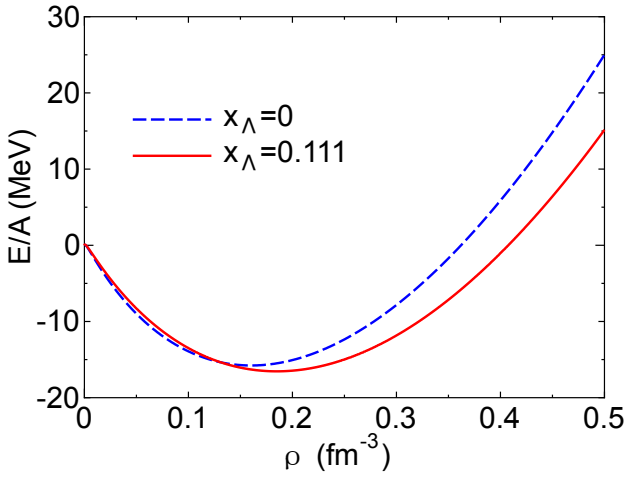

FIG. 7: (Color online) The binding energy per particle in infinite nuclear matter for the fraction of Λ particle of x_Λ=0 (the dashed line) and x_Λ=0.11 (the solid line). The neutron and the proton densities are set to be equal, that is, $\rho_n = \rho_p = (1-x_\Lambda)\rho/2$.

particle in infinite nuclear matter, E/A, given as

$$\begin{aligned}\frac{E}{A} &= \frac{H}{\rho} = \frac{H_N}{\rho} + \frac{1}{\rho}\left[\frac{\hbar^2}{2m_\Lambda}\tau_\Lambda + t_0^\Lambda\left(1+\frac{x_0^\Lambda}{2}\right)\rho_N\rho_\Lambda\right.\\ &+\frac{3}{8}t_3^\Lambda\rho_\Lambda\rho_N^2 + \frac{1}{4}(t_1^\Lambda + t_2^\Lambda)(\tau_\Lambda\rho_N + \tau_N\rho_\Lambda)\\ &+\frac{\lambda_0}{4}\rho_\Lambda^2 + \frac{1}{8}(\lambda_1+3\lambda_2)\rho_\Lambda\tau_\Lambda\\ &\left.+\frac{\lambda_3}{4}\rho_\Lambda^2\rho_N^\alpha\right], \end{aligned} \tag{20}$$

where H_N is the nucleon part of the energy density evaluated in infinite matter. ρ is the total density, while $\rho_\Lambda \equiv x_\Lambda\rho$ and $\rho_N \equiv (1-x_\Lambda)\rho$ are the densities of Λ particles and nucleons, respectively. The kinetic energy densities τ_N and τ_Λ are evaluated as $\tau_N = 3\rho_N k_{FN}^2/5$ and $\tau_\Lambda = 3\rho_\Lambda k_{F\Lambda}^2/5$, respectively, where the Fermi momenta are given by $k_{FN} = (3\pi^2\rho_N/2)^{1/3}$ and $k_{F\Lambda} = (3\pi^2\rho_\Lambda)^{1/3}$. The dashed and the solid lines in Fig. 7 show the results with the Λ fraction of x_Λ=0 and x_Λ=2/18, respectively. Here, we have assumed that the neutron and the proton densities are the same, $\rho_n = \rho_p = \rho_N/2$. One can see that the addition of Λ particles shifts the equilibrium density ρ_0 towards a high density, that is, $\rho_0 = 0.161$ fm^{-3} for x_Λ=0 and $\rho_0 = 0.185$ fm^{-3} for x_Λ=2/18. The incompressibility for infinite nuclear matter,

$$K_\infty = 9\rho_0^2\left(\frac{d^2(E/A)}{d\rho^2}\right)_{\rho=\rho_0}, \tag{21}$$

is K_∞ = 217 MeV for x_Λ=0 and K_∞ = 239 MeV for x_Λ = 2/18, agreeing with the increase of effective incompressibility of the finite hypernuclei.

Notice that this observation does not contradict to the fact that hyperons soften the equation of state for infinite nuclear matter relevant to neutron stars. That is, in neutron star calculations, the emergence of hyperons takes place at high densities and nucleons are the only constituents at the normal density, when the beta stability condition is imposed. In contrast, Fig. 7 shows the effect of hyperons on the incompressibility defined at the equilibrium density. Even though the beta stability condition does not hold there if the Λ fraction is finite, this EOS is more relevant to giant monopole resonances of finite hypernuclei.

IV. SUMMARY

We have extended the Skyrme-HF plus RPA schemes to calculations for vibrational excitations of double-Λ hypernuclei. We have applied it to the electric dipole (E1), the quadrupole (E2), and the octupole (E3) modes of excitations in the ${}^{18}_{\Lambda\Lambda}$O hypernucleus. We have shown that the strength distributions shift towards high energies for all the modes when the Λ hyperons are added to ^{16}O. This is the case both for the low-lying quadrupole and octupole states and for giant resonances. At the same time, the electromagnetic transition probabilities also decrease. We have argued that these features are mainly caused by the change in the single-particle energies, whereas the residual ΛN and ΛΛ interactions play a minor role. The calculated transition densities show that the peak of the transition densities are shifted towards inside and the height of the peaks slightly changes due to the impurity effect of Λ hyperons.

For the E1 strength, we have found a new peak at low-lying energy, that is absent in the E1 response of the core nucleus. From the analysis of the transition density, we have shown that this state corresponds to an oscillation of the Λ particles against the core nucleus.

We have also discussed the Λ-impurity effect on the isoscalar monopole vibration of ${}^{18}_{\Lambda\Lambda}$O and ${}^{210}_{\Lambda\Lambda}$Pb, and the incompressibility of infinite nuclear matter in the presence of Λ hyperons. When the Λ hyperons are added, the strength distributions are shifted to higher energies and thus the centroid energies increase, similarly to the other multipole transitions. We have shown that the transition density for the Λ particles behave rather differently from the transition densities for the neutrons and the protons. The increase of the centroid energy for the giant monopole resonance implies that Λ particles increase the nuclear incompressibility, when hyperons were emerged at the equilibrium density.

In this paper, we have studied several collective vibrational motions, taking the ${}^{18}_{\Lambda\Lambda}$O hypernucleus as examples. It would be an interesting future work to study systematically the Λ-impurity effect on the collective excitations of other double-Λ hypernuclei. In particular, the low-lying dipole mode, originated from a dipole oscillation of the Λ particles against the core nucleus, would be interesting to study. For this purpose, we would have to extend our formalism by including the pairing correlations with the quasi-particle RPA (QRPA). Another in-

teresting extension is to study the collective excitations of single-Λ hypernuclei, although the broken time-reversal symmetry will have to be taken into account correctly there.

Acknowledgments

We thank G. Colo and H. Sagawa for discussions. This work was supported by the Japanese Ministry of Education, Culture, Sports, Science and Technology by Grant-in-Aid for Scientific Research under the program number (C) 22540262.

Appendix A: Energy densities and mean-field potentials for hypernuclei

In this Appendix A, we summarize the explicit formulae for the energy densities $H_{N\Lambda}$ and $H_{\Lambda\Lambda}$ in Eq.(6) and the mean-field potentials in Eq.(7).

The energy density $H_{N\Lambda}$, due to the Skyrme-type ΛN interaction given by Eq.(1), reads [24],

$$\begin{aligned} H_{N\Lambda}(\boldsymbol{r}) &= \frac{\hbar^2}{2m_\Lambda}\tau_\Lambda + t_0^\Lambda\left(1+\frac{1}{2}x_0^\Lambda\right)\rho_N\rho_\Lambda \\ &+ \frac{1}{4}(t_1^\Lambda+t_2^\Lambda)(\tau_\Lambda\rho_N+\tau_N\rho_\Lambda) + \frac{1}{8}(3t_1^\Lambda-t_2^\Lambda)(\boldsymbol{\nabla}\rho_N\cdot\boldsymbol{\nabla}\rho_\Lambda) \\ &+ \frac{1}{2}W_0^\Lambda(\boldsymbol{\nabla}\rho_N\cdot\boldsymbol{J}_\Lambda+\boldsymbol{\nabla}\rho_\Lambda\cdot\boldsymbol{J}_N) + \frac{1}{4}t_3^\Lambda\rho_\Lambda(\rho_N^2+2\rho_n\rho_p), \end{aligned} \tag{A.1}$$

while the ΛΛ part, $H_{\Lambda\Lambda}$, originated from the ΛΛ interaction given by Eq.(3) reads[26],

$$\begin{aligned} H_{\Lambda\Lambda}(\boldsymbol{r}) &= \frac{1}{4}\lambda_0\rho_\Lambda^2 + \frac{1}{8}(\lambda_1+3\lambda_2)\rho_\Lambda\tau_\Lambda \\ &+ \frac{3}{32}(\lambda_2-\lambda_1)\rho_\Lambda\boldsymbol{\nabla}^2\rho_\Lambda + \frac{1}{4}\lambda_3\rho_\Lambda^2\rho_N^\alpha. \end{aligned} \tag{A.2}$$

Here, $\rho_b=\rho_b(\boldsymbol{r})$, $\tau_b=\tau_b(\boldsymbol{r})$, $\boldsymbol{J}_b=\boldsymbol{J}_b(r)$ are the number, the kinetic energy and the spin densities, respectively ($b=p,n$, or Λ). The indices N, p, n and Λ are the nucleon, the proton, the neutron and the Λ hyperon, respectively.

After taking variation of the energy in Eq.(4) with respect to the densities, we obtain the Skyrme-Hartree-Fock equation given by Eq.(7). The mean-field potentials in Eq.(7) are given by

$$\begin{aligned} U_{q\Lambda}(\boldsymbol{r}) &= t_0^\Lambda\left(1+\frac{1}{2}x_0^\Lambda\right)\rho_\Lambda + \frac{1}{4}\left(t_1^\Lambda+t_2^\Lambda\right)\tau_\Lambda \\ &- \frac{1}{8}\left(3t_1^\Lambda-t_2^\Lambda\right)\boldsymbol{\nabla}^2\rho_\Lambda - \frac{1}{2}W_0^\Lambda\boldsymbol{\nabla}\cdot\boldsymbol{J}_\Lambda \\ &+ \frac{1}{2}W_0^\Lambda\boldsymbol{\nabla}\rho_\Lambda\cdot(-i\boldsymbol{\nabla}\times\boldsymbol{\sigma}) + \frac{1}{2}t_3^\Lambda\rho_\Lambda(2\rho_N-\rho_q), \end{aligned} \tag{A.3}$$

$$\begin{aligned} U_{\Lambda N}(\boldsymbol{r}) &= t_0^\Lambda\left(1+\frac{1}{2}x_0^\Lambda\right)\rho_N + \frac{1}{4}\left(t_1^\Lambda+t_2^\Lambda\right)\tau_N \\ &- \frac{1}{8}\left(3t_1^\Lambda-t_2^\Lambda\right)\boldsymbol{\nabla}^2\rho_N - \frac{1}{2}W_0^\Lambda\boldsymbol{\nabla}\cdot\boldsymbol{J}_N \\ &+ \frac{1}{2}W_0^\Lambda\boldsymbol{\nabla}\rho_N\cdot(-i\boldsymbol{\nabla}\times\boldsymbol{\sigma}) + \frac{1}{4}t_3^\Lambda(\rho_N^2+2\rho_n\rho_p), \end{aligned} \tag{A.4}$$

and

$$\begin{aligned} U_{\Lambda\Lambda}(\boldsymbol{r}) &= \frac{1}{2}\lambda_0\rho_\Lambda + \frac{1}{8}(\lambda_1+3\lambda_2)\tau_\Lambda \\ &+ \frac{3}{16}(\lambda_2-\lambda_1)\boldsymbol{\nabla}^2\rho_\Lambda + \frac{1}{2}\lambda_3\rho_\Lambda\rho_N^\alpha. \end{aligned} \tag{A.5}$$

Note that the index q refers only to the proton and the neutron. The effective mass for the nucleons and the Λ hyperons in Eq. (7) are given by

$$\frac{\hbar^2}{2m_q^*} = \frac{\hbar^2}{2m_N} + \frac{1}{4}(t_1^\Lambda+t_2^\Lambda)\rho_\Lambda(\boldsymbol{r}), \tag{A.6}$$

and

$$\frac{\hbar^2}{2m_\Lambda^*} = \frac{\hbar^2}{2m_\Lambda} + \frac{1}{4}(t_1^\Lambda+t_2^\Lambda)\rho_N(\boldsymbol{r}) + \frac{1}{8}(\lambda_1+3\lambda_3)\rho_\Lambda(\boldsymbol{r}), \tag{A.7}$$

respectively.

Appendix B: ΛN and $\Lambda\Lambda$ residual interactions

The matrix elements for a particle-hole residual interaction $v_{\rm res}$ are given as[37, 38]

$$\begin{aligned} v_{ph'hp'} &= \langle p(h)^{-1}LK|v_{\rm res}|p'(h')^{-1}LK\rangle, \\ v_{pp'hh'} &= \langle p(h)^{-1}LK, p'(h')^{-1}L\bar{K}|v_{\rm res}|\rangle, \end{aligned} \tag{B.1}$$

where L is the multipolarity for the particle-hole excitations and K is its z-component. For hypernuclei, the residual interaction can be separated into two parts, $v_{\rm res}=v_{\rm res}^{b_1b_2}(N)+v_{\rm res}^{b_1b_2}(\Lambda)$, where the indices b_1 and b_2 denote p, n or Λ. The interaction $v_{\rm res}^{b_1b_2}(N)$ is due to the NN residual interaction, whose explicit form can be found in *e.g.* Refs.[51–53]. $v_{\rm res}^{b_1b_2}(\Lambda)$ is the additional term due to the ΛN and the ΛΛ residual interactions. These are given in the form of,

$$\begin{aligned} v_{\rm res}^{b_1b_2}(\Lambda) &= \delta(\boldsymbol{r}_{b1}-\boldsymbol{r}_{b2})\Big(a_{b_1b_2} \\ &+ b_{b_1b_2}\Big[\boldsymbol{\nabla}_1^2+\boldsymbol{\nabla}_2^2+\boldsymbol{\nabla}_1'^2+\boldsymbol{\nabla}_2'^2-(\boldsymbol{\nabla}_1-\boldsymbol{\nabla}_1')(\boldsymbol{\nabla}_2-\boldsymbol{\nabla}_2')\Big] \\ &+ c_{b_1b_2}(\boldsymbol{\nabla}_1+\boldsymbol{\nabla}_1')(\boldsymbol{\nabla}_2+\boldsymbol{\nabla}_2')\Big), \end{aligned} \tag{B.2}$$

where $a_{b_1b_2}$, $b_{b_1b_2}$ and $c_{b_1b_2}$ are given by

$$\begin{aligned} a_{qq'} &= \frac{t_3^\Lambda}{4}\rho_\Lambda\Big(3-\boldsymbol{\sigma}\cdot\boldsymbol{\sigma}'-\boldsymbol{\tau}\cdot\boldsymbol{\tau}'-\boldsymbol{\sigma}\cdot\boldsymbol{\sigma}'\boldsymbol{\tau}\cdot\boldsymbol{\tau}'\Big) \\ &+ \frac{\lambda_3}{4}\alpha(\alpha-1)\rho_N^{\alpha-2}\rho_\Lambda^2 \\ b_{qq'} &= c_{qq'} = 0, \end{aligned} \tag{B.3}$$

$$
\begin{aligned}
a_{\Lambda q} &= t_0^\Lambda \left(1 + \frac{x_0^\Lambda}{2}\right) + \frac{t_0^\Lambda x_0^\Lambda}{2}\boldsymbol{\sigma}_1\cdot\boldsymbol{\sigma}_2 \\
&\quad + t_3^\Lambda \left(\rho_N - \frac{\rho_q}{2}\right) + \frac{\lambda_3}{2}\alpha\rho_N^{\alpha-1}\rho_\Lambda \qquad \text{(B.4)} \\
b_{\Lambda q} &= -\frac{1}{8}(t_1^\Lambda + t_2^\Lambda), \quad c_{\Lambda q} = \frac{1}{8}(t_1^\Lambda - 3t_2^\Lambda).
\end{aligned}
$$

for $(q, q' = p \text{ or } n)$, and

$$
\begin{aligned}
a_{\Lambda\Lambda} &= \frac{1}{2}\lambda_0(1 - \boldsymbol{\sigma}_1\cdot\boldsymbol{\sigma}_2) + \frac{1}{2}\lambda_3\rho_N^\alpha(1 - \boldsymbol{\sigma}_1\cdot\boldsymbol{\sigma}_2) \\
b_{\Lambda\Lambda} &= -\frac{1}{16}\Big(\lambda_1(1 - \boldsymbol{\sigma}_1\cdot\boldsymbol{\sigma}_2) + \lambda_2(3 + \boldsymbol{\sigma}_1\cdot\boldsymbol{\sigma}_2)\Big) \qquad \text{(B.5)} \\
c_{\Lambda\Lambda} &= \frac{1}{16}\Big(\lambda_1(1 - \boldsymbol{\sigma}_1\cdot\boldsymbol{\sigma}_2) - 3\lambda_2(3 + \boldsymbol{\sigma}_1\cdot\boldsymbol{\sigma}_2)\Big),
\end{aligned}
$$

for the $\Lambda\Lambda$ terms.

[1] K. Tanida *et al.*, Phys. Rev. Lett.**86**, 1982 (2001).
[2] M. Ukai *et al.*, Phys. Rev. C**73**, 012501(R) (2006).
[3] H. Tamura *et al.*, Nucl. Phys. **A754**, 58 (2005).
[4] H. Kohri *et al.*, Phys. Rev. C**65**, 034607 (2002).
[5] M. Ukai *et al.*, Phys. Rev. Lett. **93**, 232501 (2004).
[6] H. Tamura *et al.*, Nucl. Phys. **A835**, 3 (2010).
[7] H. Nemura, Y. Akaishi, and Y. Suzuki, Phys. Rev. Lett. **89**, 142504 (2002).
[8] D.J. Millener, Nucl. Phys. **A804**, 84 (2008).
[9] A. Umeya, T. Harada, Phys. Rev. C**79**, 024315 (2009).
[10] T. Motoba, H. Bando, and K. Ikeda, Prog. Theor. Phys. **70**, 189 (1983).
[11] E. Hiyama, M. Kamimura, T. Motoba, T. Yamada, and Y. Yamamoto, Prog. Theor. Phys. **97**, 881 (1997).
[12] E. Hiyama, M. Kamimura, Y. Yamamoto, T. Motoba, and T.A. Rijken, Prog. Theor. Phys. Suppl. **185**, 106 (2010).
[13] M. Isaka, M. Kimura, A. Dote, and A. Ohnishi, Phys. Rev. C**83**, 044323 (2011).
[14] M. Isaka, M. Kimura, A. Dote, and A. Ohnishi, Phys. Rev. C**83**, 054304 (2011).
[15] M. Danysz *et al.*, Phys. Rev. Lett. **11**, 29 (1963).
[16] K. Nakazawa *et al.*, Nucl. Phys. **A835**, 207 (2010).
[17] H. Nemura, S. Shinmura, Y. Akaishi, and Khin Swe Myint, Phys. Rev. Lett., **94**, 202502 (2005).
[18] A. Gal, D.J. Millener, Phys. Lett. B**701**, 342 (2011).
[19] E. Hiyama, M. Kamimura, T. Motoba, T. Yamada, and Y. Yamamoto, Phys. Rev. C **66**, 024007 (2002); E. Hiyama, M. Kamimura, Y. Yamamoto, and T. Motoba, Phys. Rev. Lett. **104**, 212502 (2010).
[20] N. Auerbach, Nguyen Van Giai, and S.Y. Lee, Phys. Lett. **68B**, 225 (1977).
[21] N. Auerbach and Nguyen Van Giai, Phys. Lett. **90B**, 354 (1980).
[22] M.T. Lopez-Arias, Nucl. Phys. **A582**, 440 (1995).
[23] M. Martini, V. De Donno, C. Maieron, and G. Co', Nucl. Phys. **A813**, 212 (2008).
[24] M. Rayet, Ann. of Phys.**102**, 226 (1976); M. Rayet, Nucl. Phys. **A367**, 381 (1981).
[25] Y. Yamamoto, H. Bando, and J. Zofka, Prog. Theor. Phys. **80**, 757 (1988).
[26] D.E. Lanskoy, Phys. Rev. C**58**, 3351 (1998).
[27] T. Yu. Tretyakova and D.E. Lanskoy, Eur. Phys. J. A**5**, 391 (1999).
[28] H.-J. Schulze, A. Lejeune, J. Cugnon, M. Baldo, and U. Lombardo, Phys. Lett. **B355**, 21 (1995).
[29] D. Vretenar, W. Pöschl, G.A. Lalazissis, and P. Ring, Phys. Rev. C **57**, R1060 (1998).
[30] Myaing Thi Win and K. Hagino, Phys. Rev. C**78**, 054311 (2008).
[31] Myaing Thi Win, K. Hagino, and T. Koike, Phys. Rev. C**83**, 014301 (2011).
[32] B.-N. Lu, E.-G. Zhao, and S.-G. Zhou, Phys. Rev. C**84**, 014328 (2011).
[33] F. Minato, S. Chiba, and K. Hagino, Nucl. Phys. **A831**, 150 (2009); F. Minato and S. Chiba, Nucl. Phys. **A856**, 55 (2011).
[34] J.M. Yao, Z.P. Li, K. Hagino, M. Thi Win, Y. Zhang, and J. Meng, Nucl. Phys. **A868-869**, 12 (2011).
[35] E. Hiyama, Few-Body Syst. **34** 79 (2004).
[36] D. Vautherin and D.M. Brink, Phys. Rev. C**5**, 626 (1972).
[37] P. Ring and P. Schuck, *The Nuclear Many-Body Problem* (Springer-Verlag, Berlin, 1980).
[38] D.J. Rowe, *Nuclear Collective Motion* (Methuen, London, 1970).
[39] J. Bartel, P. Quentin, M. Brack, C. Guet, and H.B. Hakansson, Nucl. Phys. **A386**, 79 (1982).
[40] K. Ikeda, T. Myo, K. Kato, and H. Toki, Lecture Notes in Physics **818**, 165 (2010).
[41] J.P. Blaizot, Phys. Rep. **64**, 171 (1980).
[42] J.P. Blaizot, J.F. Berger, J. Dechargé, and M. Girod, Nucl. Phys. **A591**, 435 (1995).
[43] T. Li *et al.*, Phys. Rev. Lett. **99**, 162503 (2007); T. Li *et al.*, Phys. Rev. C**81**, 034309 (2010).
[44] E. Khan, Phys. Rev. C**80**, 011307 (2009).
[45] G. Colo, Nguyen Van Giai, J. Meyer, K. Bennaceur, and P. Bonche, Phys. Rev. C**70**, 024307 (2004).
[46] E. Khan, J. Margueron, G. Colo, K. Hagino, and H. Sagawa, Phys. Rev. C**82**, 024322 (2010).
[47] J. Piekarewicz and M. Centelles, Phys. Rev. C**79**, 054311 (2009).
[48] V.A. Dexheimer, C.A.Z. Vasconcellos, and B.E.J. Bodmann, Phys. Rev. C**77**, 065803 (2008).
[49] N.K. Glendenning and S.A. Moszkowski, Phys. Rev. Lett.**67**, 2414 (1991).
[50] Y. Sugahara and H. Toki, Prog. Theo. Phys. **92**, 803 (1994).
[51] K.-F. Liu, Zhongyu Ma, and Qingbiao Shen, Nucl. Phys. **A534**, 1 (1991).
[52] I. Hamamoto and H. Sagawa, Phys. Rev. C**60**, 064314 (1999).
[53] J. Terasaki, J. Engel, M. Bender, J. Dobaczewski, W.

Nazarewicz, and M. Stoitsov, Phys. Rev. C**71**, 034310 (2005).